CONDITIONING AND SIGNAL AMPLIFICATION STAGES FOR A SMART GAS MICROSENSOR MEMS

J. L. González Vidal
UAEH
jlvidal@uaeh.edu.mx

M. A. Reyes Barranca
CINVESTAV-IPN*mreyes@cinvestav.mx*

E. N. Vázquez Acosta
CINVESTAV-IPN
neo_wolfx@hotmail.com

Resumen

En este trabajo, el objetivo principal es el diseño de una etapa nueva de amplificación y acondicionamiento de señal utilizando opamps, la cual será utilizada con un microsensor de gas inteligente. Las dimensiones del diseño fueron calculadas en base al modelo de pequeña señal de los MOSFET. Las configuraciones del opamp se eligieron de acuerdo a los requerimientos del sensor. El sensor está hecho de una película delgada de ZnO, depositada sobre la capa superior de una microplaca caliente sobre un microfoso micromaquinado. Gracias a la integración de las etapas de acondicionamiento de señal dentro del diseño, se dice que es un sensor inteligente. Se respaldó la operación de la etapa de amplificación y de acondicionamiento de señal por medio de técnicas de análisis de estabilidad, tales como el método del lugar geométrico de raíces. Se realizaron simulaciones y graficaron diagramas de Bode del sistema.

Palabras clave: Sensor de gas, MEMS, Opamp, sensores inteligentes.

Abstract

In this work, the principal aim is the design of novel signal amplification and conditioning stages using opamps, for an intelligent gas microsensor. The design dimensions were computed based on a small signal model of a MOSFET. The necessary configurations for the opamp were chosen according to the requirements of the sensor, which means, that the input signals are taken from this one. The sensor is based on a ZnO thin film deposited on the top side of a micro hot plate located within a micromachined pit. Thanks to the integration of signal conditioning stages within the design, it is said that it is an intelligent sensor. The right operation of the amplification stage and signal conditioning is supported by means of techniques of analysis of stability like the roots locus method, and computed Bode diagrams and simulations have been developed.

Keywords**:** *Gas sensors, MEMS, opamp, smart sensors.*

1. Introduction

Today, MEMS microsensors and smart sensors have very important and multiple applications in industry, automotive sector, aeronautics, biomedicine, consumer staples, etc. The most important advantages about MEMS are: their size (they are small devices), their low power consumption, batch fabrication and very low costs. MEMS sensors make a rich design space of networked sensors viable [González, 2006], [Howe, 1996].

Intelligent microsensors have a sensing stage and a conditioning stage due to the fact that the sensing stage provides a very low current in the nanoampere range [González, 2006]. Such current is a nonlinear signal and, since it is extremely low, it is hard to be manipulated by any ordinary electronic circuitry. For this reason, it is necessary to add linearization and amplification stages within the same monolithic integrated circuit. With these stages, undesired effects in the integrated circuit can be eliminated, such as parasitic charges, interface problems, noise, among others [Vázquez, 2008].

The signal provided by the intelligent microsensor can then be converted to digital mode and then it be manipulated by a digital system or a digital computer.

2. Methods

Consider a gas microsensor which provides a small and nonlinear current signal. That signal must be amplified and linearized. With this in mind, an opamp was designed using CMOS technology.

Three-Stage Opamp

A three-stage opamp was proposed as is shown in figure 1, where the first stage, A1, is a differential amplifier. The later has an input labeled V_{di}. The second stage, A2, is the gain stage, which decreases the gain at high frequencies; and the last stage, X1, provides gain in current mode.

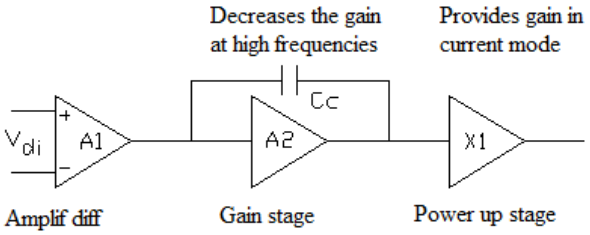

Figure 1 Three-stage opamp.

The diagram of the designed opamp is shown in figure 2. This opamp diagram was performed using Orcad® software. Subsequently, the opamp shall be explained in detail.

The Opamp design was developed according to AMIS 0.5 foundry technology and the layout was developed ~~by~~ using the L-Edit® software by Tanner-EDA. Values of $L = 2\lambda_D$, $W = 3\lambda_D$ and $\lambda_D = 1.5\ \mu m/2$ were proposed.

Differential Pair (Inputs)

To better understand how opamp works, it was divided in several parts, the first one is the differential pair input.

The differential pair is formed by M_1 and M_2 n type transistors. It is well known that the current across the differential pair, comes from a current mirror (M_3 and M_4, *p type transistors*). The dimensions of the transistors were calculated under the same conditions. That way, I_{SS} is given by equation 1.

$$I_{SS} = 10\mu A = \frac{KP_n}{2}\frac{W_{1,2}}{L_{1,2}}\left(V_{GS5,6} - V_{THN}\right)^2 \quad (1)$$

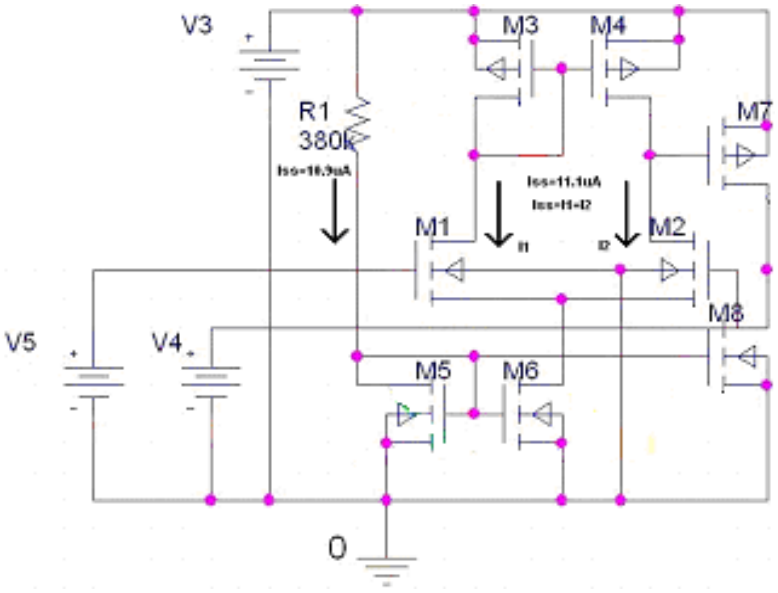

Figure 2 Opamp schematic circuit.

From equation 1 W_1=W_2=15.61 μm ≈ 21λ_D=15.75 μm and the current I_{SS}=*10.09 μA* were calculated, this current flows across M_1 and M_2. For frequency compensation, these dimensions may be increased, even when the voltage applied affects too much adversely the current value which should be a constant value. [Vázquez, 2008], [Tsivios, 1999], [Baker, 1997], [Gray, 2001].

The same design rules are now applied for p type transistors. The current source load was calculated to assure a I_{SS}=10.09μA current and a voltage of $V_{GS3,4}$=V_{THP}+0.3*V*=1.48*V*, V_{DD}=5*V*, V_{SS}=0*V*, then W_3 can be calculated using equation 2.

$$I_{SS} = 10.09\mu A = \frac{KP_p}{2}\frac{W_{3,4}}{L_3}\left(V_{GS3,4} - V_{THN}\right)^2 \quad (2)$$

W_3=W_4=52.93 μm ≈ 71λ_D=53.25 μm and I_{SS}=10.15 μA were calculated. This current parameter increases when the load potential of the current source load needs to decrease.

Current Mirror

To better understand how the differential amplifier stages work, it is necessary to understand how the current mirror works. This configuration is frequently used in circuit designing.

The current source was designed assuming that V_{DD}=5V, V_{SS}=0V, I_{SS}=10μA $V_{GS5,6}$=0.85V, with these voltage and current values both saturations of M_1 and M_2 are assured. The value of R is calculated assuming that I_{D5}= I_{D6}=10 μA, if

Solving for R, equation 3.

$$R = \frac{V_{DD} - V_{GS5,6} - V_{SS}}{I_{SS}} \tag{3}$$

Therefore, M_5 and M_6 currents have the same values; both dimensions of M_5 and M_6 were calculated by using equation 4.

$$I_{SS} = \frac{KP_n}{2}\frac{W_{5,6}}{L_{5,6}}\left(V_{GS5,6} - V_{THN}\right)^2 \tag{4}$$

Although there is a small increase in the power consumption and the gain decreases, this will not affect the designed circuit.

Output impedance is denoted by wquation 5.

$$r_o = \frac{\lambda_c}{I_D} = \frac{1}{\lambda I_D} \tag{5}$$

λ is calculated based on experimental data (0.06 V^{-1} typical), equation 6.

$$r_o = \frac{\lambda_c}{I_D} = \frac{1}{\lambda I_D} \tag{6}$$

Common Source Stage (Output)

This stage is formed with transistors M_7 and M_8. Transistor M_8 is biased as current source and the input of the amplification stage is connected to the gate of M_7.

The current through M_8 and the current mirror (M_5 and M_6) must be the same. Therefore, M_8, M_5 and M_6 have the same dimensions W_5=W_6= W_8=15.61 μm ≈ 21λ_D=15.75 μm, whereas M_7 has the same dimensions than M_8, therefore, the value of the current mirror and the differential pair is the same current.

Once the simulation is carried out, the transistor dimensions should be adjusted to fulfill the polarization requirements, signal conditioning, power consumption, stability and gain, among others [Vázquez, 2008], [Razavi, 2001], [Giurgiutiu, 2010], [Schilling, 1999].

3. Results

With the objective of determining the characteristics of the opamp, the circuit performance was simulated, 2.5 V were applied to the non-inverting input (V5) with two voltage sweeps. The first sweep is from 0 to 5 V and the second one from 2.47 V to 2.53 with 0.001 V steps in the non-inverting terminal (V4).

The diagram of opamp was simulated with Orcad® software, according to the parameters of V3.1, level 7 of AMIS 0.5μm technology libraries, equations have a complexity degree of level 3. The results from simulations are shown in figure 3, where the I_{SS} in M_5 is raised to 10.9 μA due to channel modulation effects (figure 3a), and I_{SS} in M6 is raised to 11.1 μA (figure 3b). On the other hand, voltage V_{GS} in M_5 is 858 mV (figure 3c). From figure 3d it is shown that the equation $V_{GS5} \geq 0.3V+V_{THN}$ is satisfied which means that the transistors are in saturation [Vázquez, 2008].

Gain

Gain is expressed by the equation 7.

$$A_{OL} = A_1 \cdot A_2 = g_{m1}\left(r_{o2} \| r_{o4}\right) \cdot \left[- g_{m7}\left(r_{o7} \| r_{o8}\right)\right] \tag{7}$$

From figure 4, it can be determined that the gain is given by equation 8.

$$\left|A_{OL}\right| = \frac{\Delta V_{Output}}{\Delta V_{Input}} = \frac{2.93V}{6815\,\mu V} = 4{,}305 \tag{8}$$

Gain is modified due to body effect. Gain results in the λ variation and, in consequence, the variation of equation 8. The output current of the second stage will be the same current of the design, this means I_{SS} = 10.9 μA.

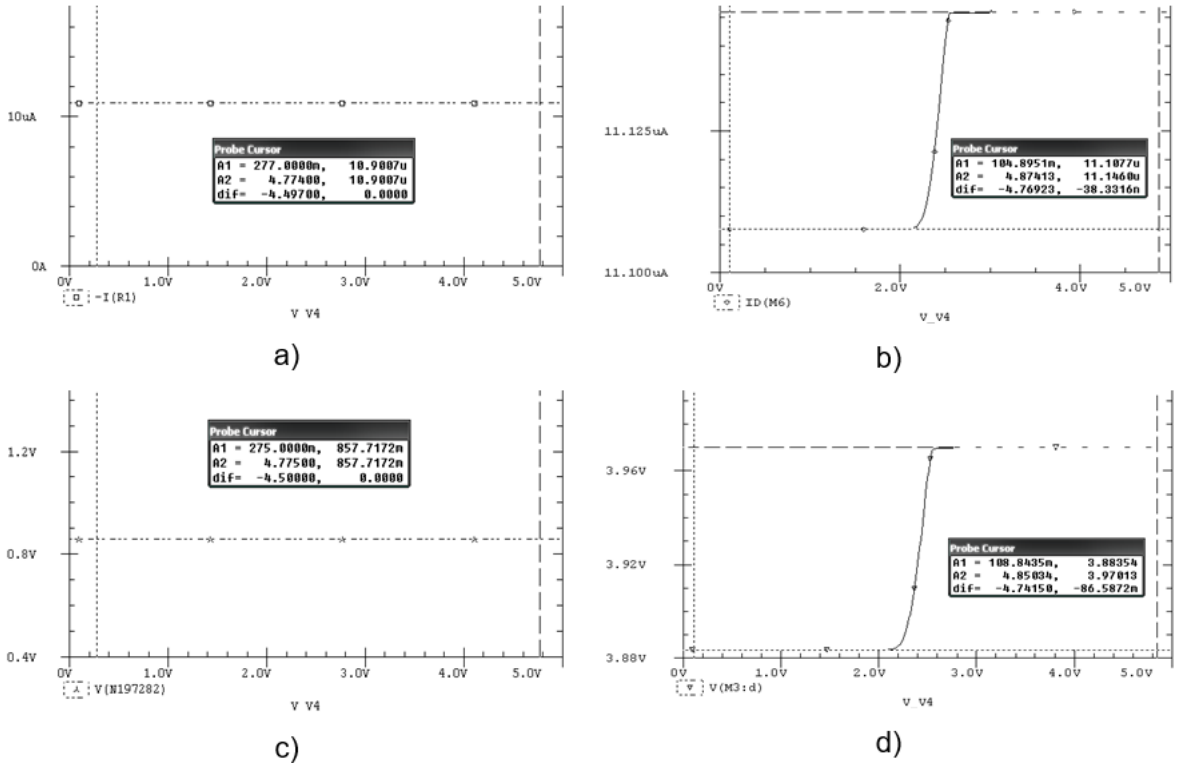

Figure 3 Simulation plots of schematic of figure 2.

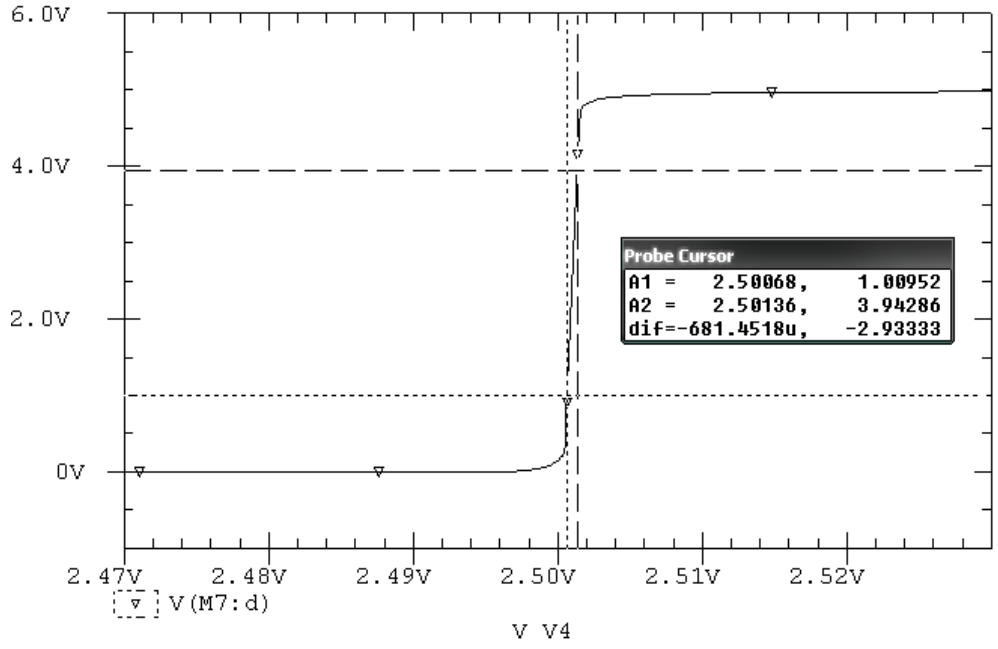

Figure 4 Opamp response due two voltage sweeps applied.

Small Signal Analysis

In a two-stage amplifier, figure 5, and considering high impedance nodes, which determine the dominant poles, the output resistance R_1 of the opamp ~~is~~ connected to ground, is given by equation 9.

$$R_1 = r_2 \| r_4 \tag{9}$$

Where both Υ_2 and Υ_4 are the output impedances of M_2 and M_4 respectively.

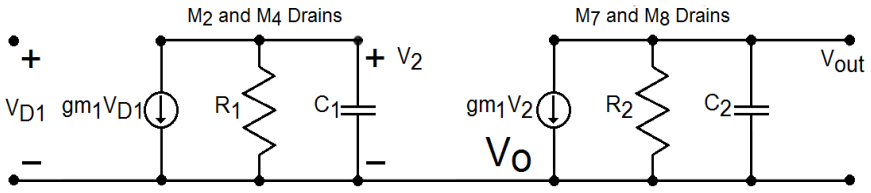

Figure 5 Small signal model of a two stages amplifier.

Capacitance C_1, can be calculated using equation 10.

$$C_{TOT} = C_L + C_{db4} + C_{gd4} + C_{db2} + C_{gd2} \tag{10}$$

Where C_{TOT} is the total capacitance of the circuit, the load capacitance C_L is C_{dg7} + C_{gs7}, which are drain-gate and gate-source capacitances of M_7, C_{db4} and C_{gd4} are drain-bulk and gate-drain capacitances of M_4, C_{db2} and C_{gd2} are drain-bulk and gate-drain capacitances of M_2. Since C_{dg7} is connected between the input and the output of the amplifier, the Miller theorem can be applied to divide the capacitance in two parts. The first capacitance is connected to the input and the second one to the output of the amplification stage. Miller capacitances are supposed to be connected to the gate and to the physical ground and between the drain and the physical ground; then, the load capacitance is now by equation 11.

$$C_L = C_{gs7} + C_{MI} \tag{11}$$

Where C_{MI} is known as Miller input capacitance, C_{MI} is denoted by equation 12.

$$C_{MI} = (1 + |A_2|) \tag{12}$$

And C_{MO}, the output miller capacitance, is denoted by equation 13.

$$C_{MO} = \left(1 + \frac{1}{|A_2|}\right) \tag{13}$$

On the other hand, the drain node of M_7 is characterized by R_2 *and* C_2, where $R_2 = R_1$, because the current of polarization is the same.

C_2 is given by equation 14.

$$C_2 = C_{gd7}\left(1 + \frac{1}{|A_2|}C_1 = 1.14\,pF\right) + C_{db7} + C_{db8} + C_{gd8} \tag{14}$$

Finally, the calculated values are $R_1 = R_2 = 1502\ k\Omega$, $C_1 = 1.14\ pF$ and $C_2 = 1.84\ fF$ [Vázquez, 2008], [Giurgiutiu, 2003].

Frequency Response Analysis

The closed-loop gain of the opamp is described in terms of equation 15.

$$A_{CL} = \frac{A_{OL}}{1 + A_{OL}\beta} \tag{15}$$

Where A_{OL} is the open loop gain of the opamp.

The amplifier reaches stability, equation 16.

$$|A_{OL}\beta| = 1 \text{ and } \angle A_{OL}\beta = \pm 180^{o} \tag{16}$$

Where β represents the amount of output signal that could be feedback and subtracted to the input of the amplifier; the highest possible value of β with amplification is given when $\beta=1$ and this condition is achieved in the voltage follower configuration.

Figure 6 shows the Bode plots resulting from the simulations. These were performed using the Orcad® software, applying an input signal of 0.01 Hz up to 10 GHz, with 10-decade steps. In figure 6a, the system shows a unit gain (0dB), which corresponds to a phase angle of 45°, whereas figure 6b shows that the gain is -25.997dB, which means that the system does not require external compensation [Vázquez, 2008], [Razavi, 2001], [Giurgiutiu, 2010], [Schilling, 1999].

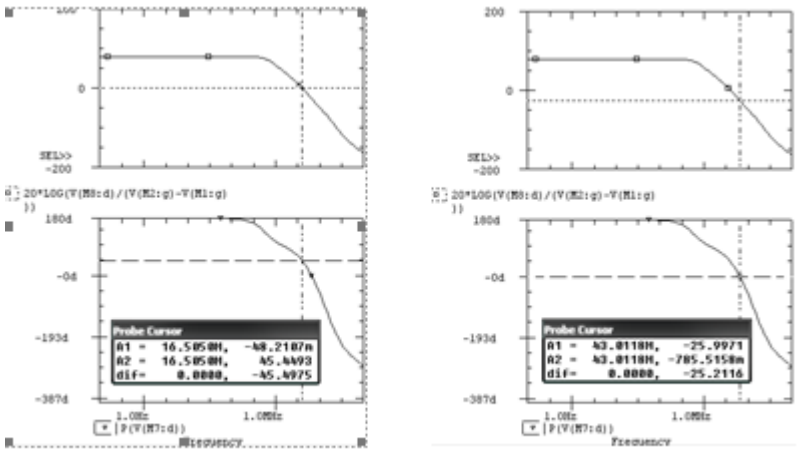

Figure 6 Bode plots.

Opamp Characterization

One quality of the opamp is to reject a common signal (CMRR) applied to its two inputs and it is represented by the gain in common mode given by equation 17.

$$CMRR = 20\log\left|\frac{A_v}{A_c}\right| = 20\log\left|g_{m1}\left(r_{o2}\|r_{o4}\right)\cdot 2g_{m4}r_{o6}\right| \tag{17}$$

In figure 7 it can be noticed that *CMRR=-42.92dB*, which is a convenient value for a good performance of the amplifier. On the other hand, the power supply rejection ratio (PSRR) is used to describe the amount of noise that a voltage power supply of a particular device can reject (equation 18).

$$PSRR = A_{OL}/(v_{out}/v_{\sin}) \tag{18}$$

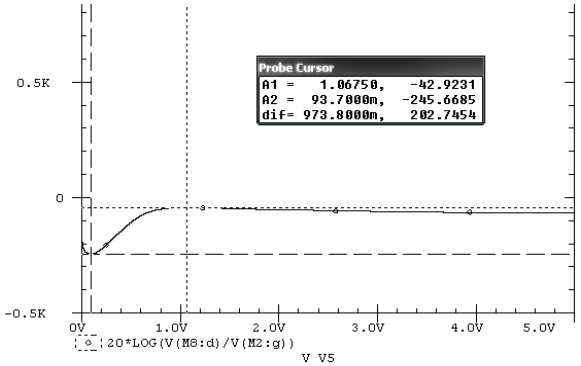

Figure 7 Common mode gain (CMRR) for an input signal applied (0 through 5 V, with 0.0001 V steps).

Where A_{OL} is the open-loop gain, v_{out} is output voltage and v_{sin} is input sinusoidal voltage; for this opamp PSRR = -3.704dB. Figure 8 shows the maximum cut frequency, where a f_{max} = 195 KHz can be noticed [Vázquez, 2008].

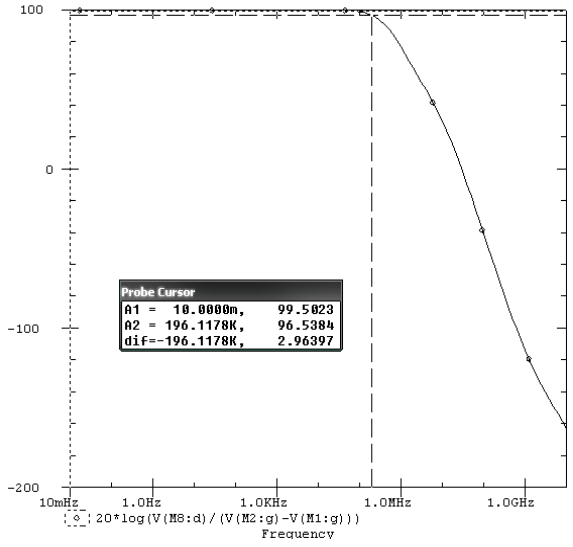

Figure 8 PSRR simulation.

Gas sensor-Opamp Connection

It is well known that electrical properties of semiconductors have a tight dependence on temperature. In the case of semiconductor oxides, a ZnO thin film must reach temperatures close to 300 ºC so the right adsorption and reduction processes can be correctly carried out in presence of oxidizing or reducing species. The main characteristic of a ZnO thin film is that the variation of its resistance is not ~~a~~ linear in presence of a reducing species such as CO. For this reason, the most of gas sensors are based on thin films of semiconductor oxides, this process is explained in detail in [González, 2005, 2006, 2013].

In figure 9, the behavior of a gas sensor can be observed. The gas sensor measurements were compared to simulations that were carried out using Matlab® and Orcad® softwares. The use of a 100MΩ resistance in series (voltage divider) with the gas sensor, allowed getting voltage values for different CO concentrations. Due to sensor resistance variation, it cannot be measured directly. For this reason, an opamp in voltage follower configuration is connected to the voltage divisor

output; this allows the interaction between the gas sensor and the load. In this case, the load is a variable gain amplifier (VGA).

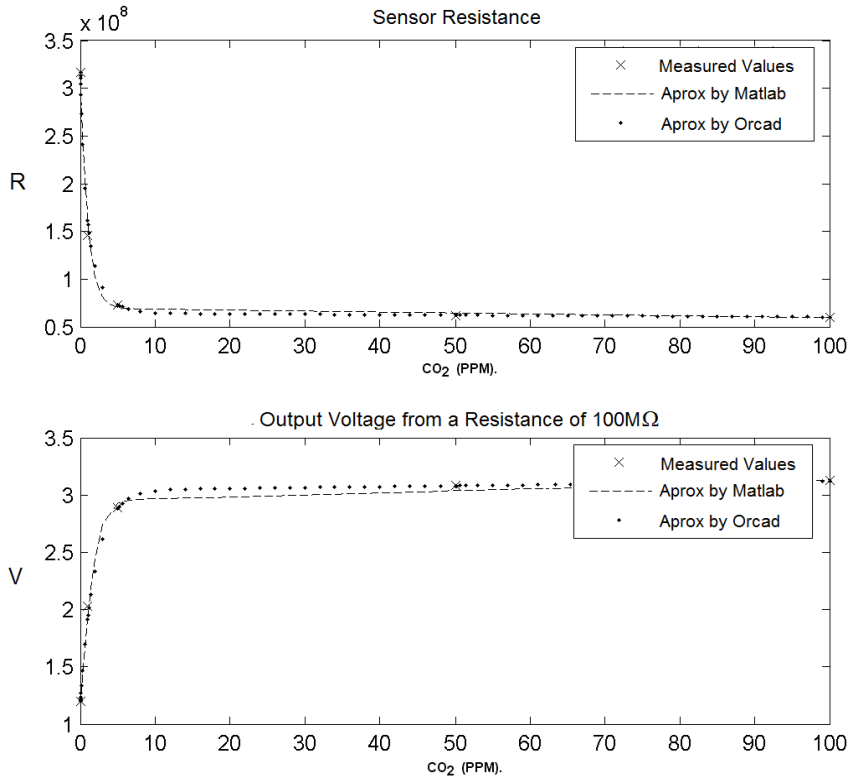

Figure 9 Variation of sensor resistance and voltage divider output potential for several CO_2 concentrations.

Since the output in voltage mode of a voltage divisor has a logarithmic behavior, an output in a proportional voltage mode of CO concentration is desired. The VGA provides a linear variation of output voltage of the signal conditioning stage, with respect to a CO concentration variation. After analyzing the slope of the logarithmic plot, there are four regions where such variation of the plot is minimum. Therefore, the VGA has four possible changes in its gain (although there might be fifteen changes). Each of the four regions already mentioned have different slopes that must be interpreted. VGA lets every region to have the same slope; nevertheless, the slope increases or decreases the voltage value in each region, which means that it moves the whole region upwards or downwards. That is why compensation voltages are required. Compensation voltages are different in each region and they

depend on the gain. Voltages are added or subtracted to a whole region depending on whether the signal is amplified or attenuated, respectively [Vásquez, 2008].

The current follower circuit is connected to the VGA output with the purpose of avoiding any interaction with the load. Figure 10 shows the schematic circuit. It was designed with connections for external resistances, because external resistances can modify the gain. First and third terminals are designed for power supply connection. The second terminal is designed for connection of the 100 MΩ resistance, V_{div} is the output voltage of A_{s1}; an input resistance R_1 is connected to V_{div} and R_1 terminals; V_c is the voltage that compensates the gain change of A_{gv}; $C_{V1,2,3,4}$ are control signals which determine feedback resistance. Feedback resistances R_f are connected between $R_{f1,2,3,4}$ and V_{fb}. The output signal of A_{gv} is connected to the non-inverting output of the current follower A_{s2}. A_{s2} avoids the load to drain current to A_{gv}, and finally V_{out} is the output voltage of the circuit [Vázquez, 2008].

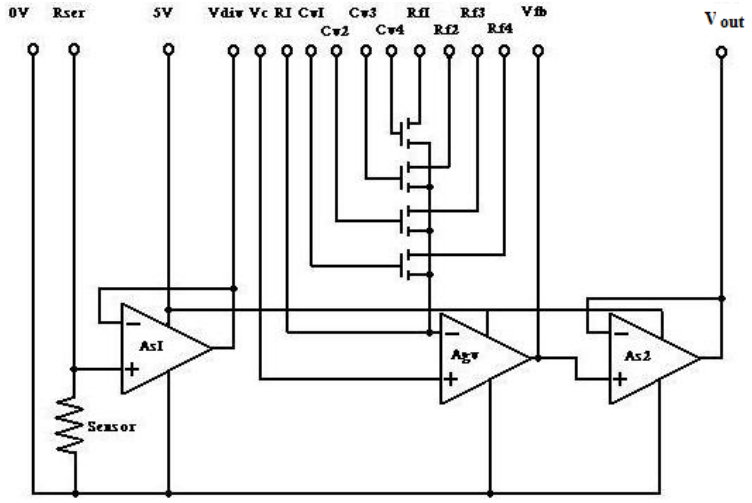

Figure 10 Schematic circuit developed.

4. Discussion

The signal conditioning stage is very important, because sensor signal linearization is needed. The sensor's linear signal is taken to a standard range for right measurements. Signal conditioning stages must have a right approximation of the sensor's behavior. The approximations were developed by Matlab® using

recursive gradient method. However, Orcad® allows designing more accurate functions for the electrical behavior of the device, because resistive, capacitive and inductive elements are used. Nevertheless, the functions developed in Matlab® had problems when they were translated to Orcad®.

On the other hand, the use of PMOS instead of NMOS makes all the transistors not to work in a saturation mode, and it was observed that their behavior was unstable. The use of a logarithmic conditioning stage does not work because the constants defined in this stage are different from the sensor's response parameters; therefore, they do not eliminate each other. Finally, using a resistance of 100MΩ in series with the gas sensor allows obtaining voltage values for different CO concentrations. Since the sensor resistance variation cannot be measured directly, an opamp in current follower configuration is connected to the voltage divisor output, and generating the possibility of interaction between the gas sensor and the load. In this case, the load is a VGA. The realization of this on-chip device will be developed.

5. Conclusions

A three-stage opamp was designed, such stages are three opamps called A1, A2 and X1; since this circuit will have a special application, a lot of values were computed.

In realizing of the opamp design, it was divided in a differential pair (formed by M_1 and M_2 transistors), current load source (formed by M_3 and M_4 transistors), current mirror (formed by M_5 and M_6 transistors) and common source stage (formed by M_7 and M_8 transistors). Drain currents I_D and transistor dimensions as W and L were calculated. Opamp design was developed according to 0.5μm AMIS technology and the layout was developed by using L-Edit software by Tanner EDA. Simulations were developed using Matlab® and Orcad® softwares. Several characteristics of the opamp were analyzed, such as gain, small signal analysis, frequency response analysis; in addition, CMRR and PSRR were calculated.

Opamp design and calculations were based on basis of semiconductors, electrical physics, magnetism concepts, modeling and transistors performance. In addition,

frequency stability was applied. Computational techniques gave us a very reliable approximation of the performance and behavior of the opamp. The designed Opamp was developed according to a particular gas sensor whose surface resistance varies two orders of magnitude.

Acknowledgments

This work was sponsored by UAEH.

6. Bibliography and References

[1] Behzad Razavi, Design of Analog CMOS Integrated Circuits, McGraw-Hill Higher Education, 2001.

[2] Donald L. Schilling, Charles Belove, Tuvia Apelewicz, Raymond J. Saccardi, Electronic Circuits, Discrete and Integrated, Third Edition, McGraw-Hill Book Company, 1999.

[3] Edgar Norman Vázquez Acosta, Diseño de etapa de amplificación y conversión A/D en un circuito integrado para un microsensor de gases (MEMS) inteligente. Master degree Thesis, UAEH, Mineral de la Reforma, Hidalgo, Mexico, 2008.

[4] J. L. González Vidal, Alfredo Reyes Barranca y Wilfrido Calleja Arriaga, Technological Processes for Micro-Heater and Micro-Hot-Plate in the Implementation of a MEM Gas Sensor, 2nd International Conference on Electrical and Electronics Engineering (ICEEE) and XI Conference on Electrical Engineering, Mexico City, Mexico, pp. 440-443, 2005.

[5] J. L. González-Vidal, Alfredo Reyes Barranca, Wilfrido Calleja Arriaga, Juan Silva F e I. Juárez, Caracterización de la interfase de Polisilicio-ZnO, para un microsensor de gases micromaquinado, XXV Congreso Nacional Sociedad Mexicana de Ciencia y Tecnología de Superficies y Materiales, Zacatecas, Zacatecas, Mexico. September 2005.

[6] José Luís González Vidal, Aplicación de Estructuras Micro-Electro-Mecánicas (MEMS) con Tecnología CMOS para Sensores de Parámetros Físicos. Ph D. Thesis, CINVESTAV-IPN, Mexico City, Mexico, 2006.

[7] Paul R. Gray, Robert G. Meyer, Analysis and Design of Analog Integrated Circuits. Wiley and Sons, 2001.

[8] R Jacob Baker, Harry W. Li and David E. Boyce, CMOS Circuit Design, Layout, and Simulation, Willey-IEEE PRESS, 1997.

[9] Roger T. Howe, Charles G. Sodini, Microelectronics, an Integrated Approach, Prentice Hall, pp 176-179, 1996.

[10] Victor Giurgiutiu, Sergey Edgard Lyshevsky, Micromechatronics. Modelling, Analysis, and Design with MATLAB®, CRC PRESS, 2003.

[11] Yannks P. Tsiviois., Operation and Modeling of the MOS Transistor, 2nd ed, Oxford University press, 1999.